

Faculty of Engineering
Faculty of Engineering - Papers

University of Wollongong

Year 2005

Development of an Equivalent
Homogenous Fluid Model for
Pseudo-Two-Phase (Air+Water) Flow
through Fractured Rock

J. Price* B. Indraratna†

*University of Wollongong

†University of Wollongong, indra@uow.edu.au

This article was originally published as price, J and Indraratna, B, Development of an Equivalent Homogenous Fluid Model for Pseudo-Two-Phase (Air+Water) Flow through Fractured Rock, *Journal of Geotechnical and Geoenvironmental Engineering*, 131, July 2005, 857. Copyright American Society of Civil Engineers. Original journal available <[a href="http://scitation.aip.org/gto" >here](http://scitation.aip.org/gto).

This paper is posted at Research Online.

<http://ro.uow.edu.au/engpapers/109>

Development of an Equivalent Homogenous Fluid Model for Pseudo-Two-Phase (Air+Water) Flow through Fractured Rock

J. Price¹ and B. Indraratna²

Abstract: Fracture flow of two-phase mixtures is particularly applicable to the coal mining and coal bed methane projects in Australia. A one-dimensional steady-state pseudo-two-phase flow model is proposed for fractured rock. The model considers free flow of a compressible mixture of air and water in an inclined planar fracture and is based upon the conservation of momentum and the “cubic” law. The flow model is coupled to changes in the stress environment through the fracture normal stiffness, which is related to changes in fracture aperture. The model represents the individual air and water phases as a single equivalent homogenous fluid. Laboratory testing was performed using the two-phase high-pressure triaxial apparatus on 54 mm diameter (approximately 2:1 height:diameter) borehole cores intersected by induced near-axial fractures. The samples were of Triassic arenaceous fine-medium grained sandstone (known as the Eckersley Formation) that is found locally in the Southern Coalfield of New South Wales. The sample fracture roughness was assessed using a technique based upon Fourier series analysis to objectively attribute a joint roughness coefficient. The proposed two-phase flow model was verified using the recorded laboratory data obtained over a range of triaxial confining pressures (i.e., fracture normal stresses).

DOI: 10.1061/(ASCE)1090-0241(2005)131:7(857)

CE Database subject headings: Two phase flow; Rocks; Fracture; Coal mining; Triaxial tests.

Introduction

Two-phase flow through fractured geological media is an aspect of hydromechanics that is of increasing importance in the fields of civil construction as well as resource storage and extraction. Geotechnical analysis of this problem is very difficult to undertake because of the dynamic and complex interaction of fluid phases as well as the irregular natural fracture topology. The concept of a single-homogenous fluid, equivalent to that of the two separate phases, has allowed simplifications to be applied to the accepted theory, in order to approximate the flow of mixed fluids through fractured geological media. Previous applications of this approach have used relatively smooth surfaces (Fourar et al. 1993) or surfaces of unknown roughness (Persoff and Pruess 1993). The approach applied in this current study enables the impact on flow of surface roughness and aperture variation to be carefully considered. Work performed as part of this research project has identified the fracture roughness of the test specimens so that the impact of friction losses can be isolated from mechanical effects, such as the closure of the fracture aperture due to an increase in

stress. The proposed theoretical model has been validated by comparing the results of laboratory tests using a two-phase high-pressure triaxial apparatus (TPHPTA) with the predicted behavior.

Theoretical Model

Arguably, the most convenient approach to the analysis of two-phase fluid mixtures flowing in natural rock fractures is that of the homogenous fluid model. The advantages of this macroscopic model include removing the need for information on the rate of phase change within the fracture, knowledge of the localized microscopic flow behavior (e.g., individual bubble flow path) and particular knowledge of the specific two-phase flow pattern present under the instantaneous phase velocity and pressure drop conditions. The proposed technique considers the free flow of water and gas phases through the fracture, and is based upon estimated homogenous fluid properties calculated from the relative combination of the separate fluid phases. The model is constrained by the following assumptions and limitations.

- (1) The aperture and fluid pressure gradients are large enough so that interfacial capillary pressures between opposing fracture surfaces and elevation gradient across the fracture length are negligible.
- (2) The model is limited to the analysis of a bubble mixture and considers the motion of air bubbles entrained in a continuous water phase, such that phase velocities are effectively equal.
- (3) The fracture walls remain wetted because of the capillary pressures associated with the rough fracture surface and the small matrix pore size.
- (4) The rock is “hard” with deformation approximated as linear elastic within the observed normal stress ranges. In this case, fracture deformation is more sensitive to changes in normal stress than changes in fluid pressure.

¹Doctoral Candidate, School of Civil Engineering, Univ. of Wollongong, Northfields Ave., Wollongong, NSW 2522, Australia.

²Professor, School of Civil Engineering, Univ. of Wollongong, Northfields Ave., Wollongong, NSW 2522, Australia. E-mail: indra@uow.edu.au

Note. Discussion open until December 1, 2005. Separate discussions must be submitted for individual papers. To extend the closing date by one month, a written request must be filed with the ASCE Managing Editor. The manuscript for this paper was submitted for review and possible publication on April 12, 2004; approved on September 25, 2004. This paper is part of the *Journal of Geotechnical and Geoenvironmental Engineering*, Vol. 131, No. 7, July 1, 2005. ©ASCE, ISSN 1090-0241/2005/7-857-866/\$25.00.

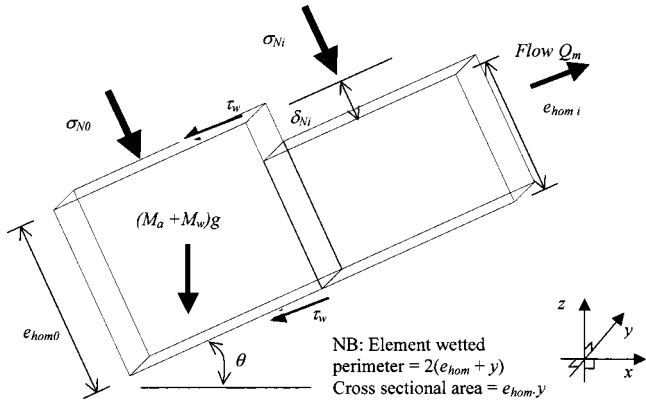


Fig. 1. Schematic section of joint element at time zero (left) and time t (right) following the application of incremental fracture normal stress $\Delta\sigma_N$

(5) The primary permeability of the rock substance is negligible. Fig. 1 shows a simplified three-dimensional (3D) smooth joint element of aperture e (such that $e_{\text{hom}} = E_{\text{mech}}$) inclined at an angle θ , at time $t=0$, and at time $t=i$, following a normal stress increment $\Delta\sigma_N$. Using the proposed approach, the basic one-dimensional form of the equations for continuity and the conservation of momentum for steady-state isothermal flow can be written in the following forms for a fracture (after Wallis 1969):

$$M = \rho_m v A = \text{constant} \quad (1)$$

$$M_m \frac{dv}{dx} = -A \frac{du}{dx} - P\tau_w - A\rho_m g \sin \theta \quad (2)$$

where M_m =total mass flow rate ($M_a + M_w$) of Phases a and b (kg s^{-1}); ρ_m =mixture density (t m^{-3}); A =cross-sectional fracture area (m^2), i.e., the product of fracture aperture and width ($e \cdot y$); P =fracture wetted perimeter (m); v =flow velocity (m s^{-1}); u =fluid pressure (kPa); and τ_w =average shear stress acting on the fracture wall (kN m^{-2}). These terms are also defined in Fig. 1.

The Continuity Eq. (1) defines the mass flux of the fluid which remains the same despite changes in phase volume that may result from the change in stress or changes in aperture. Eq. (2) can be rearranged to express the total pressure gradient acting across the rock fracture (du/dx), in terms of losses due to friction, acceleration and gravitational potential referring, respectively, to the three right-hand terms of Eq. (3):

$$\frac{du}{dx} = -\frac{P}{A}\tau_w - \frac{M_m}{A} \frac{dv}{dx} - \rho_m g \sin \theta \quad (3)$$

In the case of the testing followed in this study, it is contended that the gravitational terms can be effectively ignored since the change in elevation is equivalent to between 5% and 0.5% of the pressure drop. For smaller pressure drops, gravity and capillary forces will have a greater impact on the flow and should be included in the calculations.

The average shear stress acting on the fracture wall due to the flow of the mixture can be written in terms of a friction factor (C_f):

$$\tau_w = 0.5C_f \rho_m v^2 \quad (4)$$

where C_f is defined empirically using the Reynolds number for the mixture R_m in accordance with Fourar et al. (1993) for laminar flow as $68.06/R_m^{1.1}$ and $6.46/R_m^{0.61}$ for smooth and rough frac-

tures, respectively. This finally allows the frictional pressure gradient term for a smooth planar fracture of unit width ($y=1$) to be written as

$$\left(\frac{du}{dx}\right)_F = \frac{P}{A}\tau_w = \left(\frac{1}{e} + 1\right)C_f M_m Q_m \quad (5)$$

where Q_m =total mixture flow rate ($Q_a + Q_w$). The pressure gradient due to changes in acceleration can be written as

$$\left(\frac{du}{dx}\right)_A = \frac{M_m}{A} \frac{dv}{dx} = \frac{M_m}{A} \frac{d}{dx} \left(\frac{M_m}{A\rho_m}\right) \quad (6)$$

Substituting Eqs. (5) and (6) in Eq. (3) gives the following equation:

$$\frac{du}{dx} = -\left(\frac{1}{e} + 1\right)C_f M_m Q_m - \frac{1}{e^2} M_m^2 \frac{d}{dx} \left(\frac{1}{\rho_m}\right) - \rho_m g \sin \theta \quad (7)$$

The homogenous fluid properties used in this work are expressed in terms of the phase flows ($Q_i, \text{m}^3 \text{s}^{-1}$), the mass flow rate (M_i), and corresponding phase density (ρ_i), such that the mixture density (ρ_m) is given by

$$\rho_m = \frac{1}{Q_m} (\rho_a Q_a + \rho_w Q_w) \quad (8)$$

The mixture viscosity ($\mu_m, \text{kPa s}$) is defined according to the work of McAdams et al. (1942), in terms of the mass fraction of the phase flows:

$$\mu_m = M_m \left(\frac{\mu_a}{M_a} + \frac{\mu_w}{M_w} \right) \quad (9)$$

As is often the case in hydromechanical problems, the combination of Poiseuille's and Darcy's law is considered applicable to analyzing laminar homogenous fluid flows for small pressure gradients:

$$Q_m = \frac{e_{\text{hom}}^3 y}{12\mu_m} \left(\frac{du}{dx} + \rho_m g \frac{dz}{dx} \right) \quad (10)$$

where e_{hom} is the back-calculated fracture aperture based upon a homogenous fluid.

When a fracture is acted upon by a change in normal stress $\Delta\sigma_N$, the resulting change in fracture aperture δ_N , is counteracted by compression of the fluid mixture. For single-phase flows of compressible liquids, the fluid can be regarded as effectively incompressible, whilst the relative velocity of the two phases is small (Vennard and Street 1982). When considering a homogenous fluid comprised of gas and liquid, it is assumed that the resulting mixture has a compressibility related to the relative proportions of each of the individual phases and the changes in stress at the macroscopic mechanical level.

Indraratna and Ranjith (2001a) found that the total normal deformation (Δ_T) of the fracture aperture can be related to the compressibility of air (ξ_{ac}) and water (ξ_{wc}), the solubility of air in water (ξ_{ad}), and the mechanical normal deformation (δ_N) due to changes in stress. Hence

$$\Delta_T = \xi_{ac} + \xi_{ad} + \delta_N - \xi_{wc} \quad (11)$$

When considering a homogenous fluid, this expression simplifies to

$$\Delta_T = \delta_N - \xi_{mc} \quad (12)$$

where ξ_{mc} =volumetric compression (ΔV) of the homogenous fluid mixture per unit fracture area. The compressibility of the

mixture is comprised of the compression of the air and water phases under the local phase pressure. As the water phase is relatively stiff, most of the compression is accommodated by the air phase. The negative sign for ξ_{wc} allows for the air phase to expand to occupy any compression of the water phase. Hence, for a fracture of length ℓ and unit width, inclined at θ to the horizontal, the compression can be written as

$$\xi_{mc} = \frac{\Delta V}{\ell^2 \cos \theta \sin \theta} \quad (13)$$

The isothermal compressibility of air and water (C_a and C_w) can be used to calculate the compressibility of an air-water mixture based upon the volumetric composition of both phases. The compressibility of the individual phases can be written in the form of

$$C_w = \frac{1}{V_w} \frac{dV_w}{du_w} \quad (14)$$

Thus, for an air-water mixture, the compressibility is given by

$$C_{aw} = \frac{1}{V_a} \frac{dV_a}{du_a} + \frac{1}{V_w} \frac{dV_w}{du_w} \quad (15)$$

If the total fracture volume, $V = V_a + V_w$, and then considering the wetting phase saturation (S_w) to make the air phase volume $V_a = V(1 - S_w)$, Eq. (15) can be rewritten to include the change in pore phase pressure with respect to total stress change ($du_i/d\sigma$), after Fredlund and Rahardjo (1993):

$$C_{aw} = \frac{1}{V_w + V_a} \left(\frac{dV_a}{du_a} \frac{du_a}{d\sigma} + \frac{dV_w}{du_w} \frac{du_w}{d\sigma} \right) \quad (16)$$

The differential can be expanded so that compressibility is a function of the water phase saturation and the phase compressibility:

$$C_{aw} = C_a(1 - S_w) \frac{du_a}{d\sigma} + C_w S_w \frac{du_w}{d\sigma} \quad (17)$$

Rewriting Eq. (13) with the preceding terms gives:

$$\xi_{mc} = \frac{\Delta V}{\ell^2 \cos \theta \sin \theta} = \frac{V_a + V_w}{\ell^2 \cos \theta \sin \theta} \left(C_a(1 - S_w) \frac{du_a}{d\sigma} + C_w S_w \frac{du_w}{d\sigma} \right) \quad (18)$$

The fluid under test is conceptualized as gas bubbles mixed within a continuous water phase. In the test fracture, the independently injected air and water pressures are envisaged to rapidly equilibrate through localized changes in phase saturation (S_i). In this case, where the difference in elevation across the fracture is small and interphase slip is negligible, one can assume $du_a = du_w = du$.

The change in fracture aperture is related to the normal fracture stiffness (K_N) and the change in applied normal stress ($\Delta\sigma_N$). An equation can be written in terms of effective stress, since the mechanical reaction of a water-filled fracture will be mitigated by the presence of the fluid mixture with a pore pressure u . For a coordinate system where principal maximum and minimum stresses are parallel to the z and x axes, respectively, the expression is given by:

$$\delta_N = \frac{\Delta\sigma'_N}{K'_N} = \frac{\Delta\sigma_N - \Delta u}{K'_N} = \frac{\Delta(\sigma_1 \cos^2 \theta - \sigma_3 \sin^2 \theta) - \Delta u}{K'_N} \quad (19)$$

The change in fracture normal stiffness can be assessed from test observations of clip gauge deflection with changes in confining stress and pore fluid pressure. The fluid mixture within the frac-

ture will respond to the change in stress by a change in volume defined by the fluid mixture compressibility. This mixture compressibility was expressed in Eqs. (12) and (13), and is equivalent to the change in solubility of the air phase within the water, the change in the dissolved air content of the water, and the compression of the air and water phases. This allows the expression for the total fracture deformation (Δ_T) in Eq. (12) to be written as

$$\Delta_T = \frac{\Delta\sigma_N - \Delta u}{K'_N} + \frac{V_a + V_w}{\ell^2 \cos \theta \sin \theta} \left(C_a(1 - S_w) \frac{du_a}{d\sigma} + C_w S_w \frac{du_w}{d\sigma} \right) \quad (20)$$

The cubic law assumes that the flow occurs between two smooth parallel surfaces. Calculating the flow rate through a natural fracture when considering the reality of variable aperture means that for relatively rough surfaces, the calculated flow rate will be underpredicted. The effect of variable aperture is to promote rotational and nonparallel flow. Any assessment of the flow reduction requires that a detailed mapping of the fracture topology be available, so that the aperture characteristics can be calculated. In earlier publications (Yang and Di 2001; Indraratna et al. 2002, 2003), the Fourier series has been successfully applied to replicate fracture surfaces whereby:

$$f(x) = \frac{a_0}{2} + \sum_{n=1}^{\infty} \left(a_n \cos \frac{n\pi x}{L} + b_n \sin \frac{n\pi x}{L} \right) \quad (21)$$

$$a_n = \frac{1}{L} \int_0^{2L} f(x) \cos \frac{n\pi x}{L} dx \quad (22)$$

$$b_n = \frac{1}{L} \int_0^{2L} f(x) \sin \frac{n\pi x}{L} dx \quad (23)$$

where $f(x)$ = fracture surface elevation measured at a distance x along a fracture profile of length $2L$; n = harmonic frequency; a_n and b_n = Fourier coefficients. If two opposing fracture surfaces are both defined by separate Fourier series— $f(x)_{\text{upper}}$ and $f(x)_{\text{lower}}$ —the fracture aperture $\Phi(x)$ can equally be defined by a third Fourier series, such that

$$\Phi(x) = f(x)_{\text{upper}} - f(x)_{\text{lower}} \quad (24)$$

Combining Eqs. (10), (20), and (24), the mixture flow rate expected from a smooth fracture following a change in normal stress $\Delta\sigma_N$ would be

$$\sum_{i=a,w} Q_i = \frac{[\Phi(x) - \Delta_T]^3 y}{12\mu_m} \frac{du}{dx} \quad (25)$$

Application to Laboratory Test Results

The verification of the proposed two-phase model and the assessment of the role of roughness flow behavior requires two distinct phases of experimental study: (1) The measurement of the fracture hydromechanical properties using the TPHPTA; and (2) the detailed measurement of the fracture topology using a high-resolution 3D laser scanner to assess the fracture roughness.

Two-Phase High-Pressure Triaxial Apparatus

The TPHPTA was developed recently by researchers at Wollongong as described elsewhere in the literature (Indraratna and

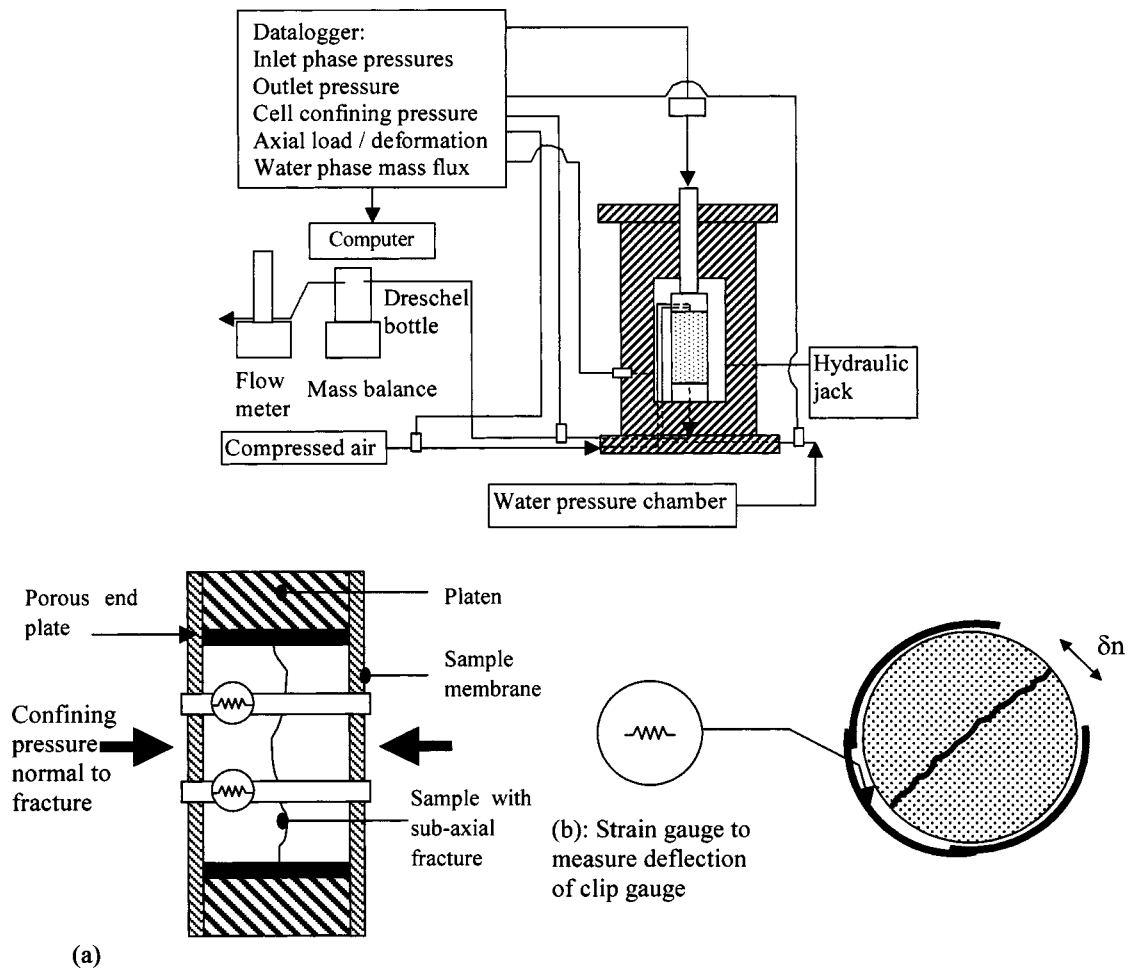


Fig. 2. Sketch diagram of two-phase high pressure triaxial apparatus with inset (a) details of test specimen encircled by two clipgauges to measure change in fracture aperture and (b) showing positioning of clip gauge around membrane and sample to measure fracture normal deflection (δ_N) during triaxial testing

Haque 1999; Indraratna and Ranjith, 2001a,b). The apparatus has since been improved so that air flow is recorded using digital flow controllers, and the mass flow of water is measured on an electronic balance that directly records the measured data to a computer at user-specified time intervals. The apparatus is shown in Fig. 2, with inset details of the sample assembly [Fig. 2(a)] and the clip gauge setup [Fig. 2(b)]. The test equipment is monitored using a DataTaker DT500 that is administered from a workstation using *DELOGGER* version 4.1 (DataTaker Pty Ltd., Victoria, Australia). The equipment subjects a 54 mm diameter sample (2:1 height:diameter) to a controlled hydrostatic stress environment using a system of hydraulic jacks to apply axial and triaxial confining stress. The confining pressure (σ_N) is monitored by a UCC 10 MPa pressure transducer. The triaxial cell is placed in a 500t capacity load frame that is loaded hydraulically and monitored using a 5t load cell.

The test procedure applies a constant nominal axial stress (σ_3) with the major principal stress (σ_1) applied effectively perpendicular to the fracture by the triaxial cell confining pressure. The sample is intersected by a subaxial fracture, and a fluid mixture of air and water is injected into the base of the sample under a measured pore pressure gradient. The fluid phases are injected independently into the base of the sample through a porous plate. The outlet phase pressure (u_{out}) of the mixture and the inlet phase pressures (u_a for air and u_w for water) were measured using UCC

5 MPa pressure transducers with nonreturn valves built into the fluid injection lines to prevent back flow of phases through the system. The dilation of the sample was measured using two spring steel clip gauges fitted with a strain gauge and mounted circumferentially around the sample. Changes in clip gauge output were used to calculate the average (fracture) normal deformation (δ_N). The gauges were monitored directly by the datalogger.

The sample was maintained at a steady confining stress and water phase pore pressure conditions during each stage of the test. Tests were performed using an incremental range of confining stress (i.e., acting perpendicular to the fracture, σ_N) from 500 kPa to about 4 MPa. The sample membrane was found to puncture locally on the sharp edges of the fracture at elevated confining stresses which truncated the range of stress conditions that could be applied to some samples.

During the test, inlet pore pressures up to about 200 kPa were applied in order to observe the flow characteristics of the fracture for flow regimes (equivalent to hydraulic gradients in the range of 100 kPa/m to 2 MPa/m). Water flow rate was calculated from mass flux measurements made using a AMD GPK12000 mass balance (accuracy ± 0.01 g) connected directly to the laboratory computer serial port and set up to report data coincidentally with the DT500 datalogger. Air flow rate was recorded using Dwyer Digital GFC 0–500 ml/min and 0–30 l/min flow controllers connected to the DT500 to record instantaneous flow.

For each stage of the test, under single-phase conditions an initial water inlet pressure was applied until steady-state water flow was achieved. The air phase pressure was then introduced and increased incrementally until steady-state two-phase flow conditions were again re-established, while recording the separate phase flow rates and the inlet and outlet phase pressures. The test methodology was repeated at an increased triaxial confining stress, so that the hydromechanical behavior of the fracture could be studied using sample deformation data collected from clip gauges located circumferentially around the sample. The parameter E_{clip} represents the average mechanical aperture calculated from the initial mechanical aperture E_{mech0} minus the clip gauge deformation δ_N due to an incremental fracture normal stress. E_{mech0} is the average lognormal aperture calculated from analysis of laser scanning data previously, corresponding to zero-normal stress conditions.

Roughness Measurement

Surface roughness data were acquired using a Minolta Vivid 910 High-Resolution noncontact 3D Laser Scanner. The sample was placed in a cradle with the fracture plane approximately perpendicular to the axis of the laser. Laser power and focal length settings were finely adjusted to optimize data recovery and to minimize the number of “fly-off” data points (i.e., minimize error). Scans were automatically recorded at 0.1 mm intervals in the fracture plane to a vertical (z plane) precision of ± 0.008 mm. The scanned coordinate data were saved in ASCII format allowing data processing and analysis. The surface roughness methodology is described elsewhere (Indraratna et al. 2002; Price 2005). A simple manipulation of the data allowed the calculation of the physical or “mechanical” aperture \bar{E}_{mech} . The methodology involves a silastic or resin mold being made of the fracture aperture by injecting the compound between the two mated fracture surfaces. Once the molding material has set, one-half of the fractured sample is removed and the exposed mold surface scanned. The molding is then carefully removed and the remaining fracture half is scanned using the same coordinate system and scan interval. Subtraction of the elevation readings for each data point generates a set of mechanical or “physical” aperture values across the sample. The molding represents the aperture geometry when the fracture is confined only by the weight of the overlying half of the fracture. For a cylindrical sample 110 mm high, the weight of one-half of the sample acting normally at the fracture plane would be equivalent to a stress of less than 1 kPa. The small magnitude of this normal stress means that the situation is effectively the same as a zero-confining stress condition. The histogram of the fracture data (Fig. 3) shows an approximately log-normal distribution. The average log-normal aperture E_{log} was calculated from the exponent of the average log-aperture value and also represents the average mechanical aperture at zero-normal stress E_{mech0} .

In addition to stress-related aperture dilation, the surface roughness must be estimated so that the approximation of the flow to the idealized parallel-plate conditions can be evaluated. The reduction of single-phase flow by increasing surface roughness for particular fluids is clearly established throughout published literature (e.g., Witherspoon et al. 1981), whereby the intrinsic permeability could be reduced by up to five orders of magnitude, when comparing the theoretical parallel-plate aperture with that calculated from the Barton et al. (1985) relationship Eq. (26):

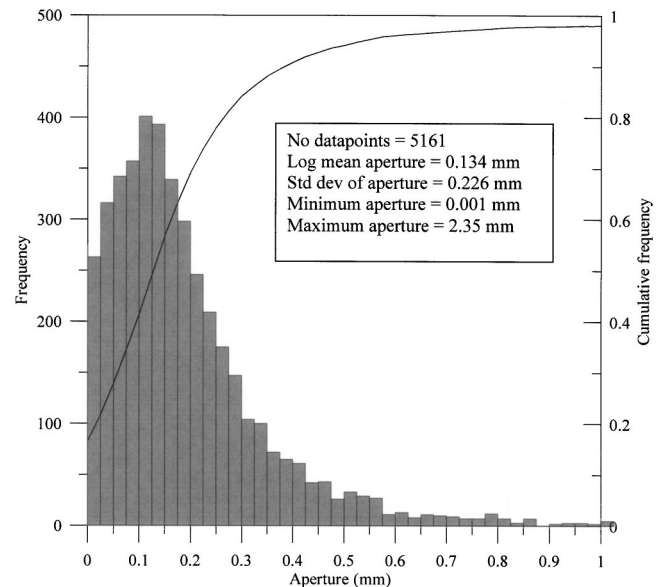


Fig. 3. Statistical analysis of data set from laser scanning of Sample JP09

$$e = \frac{E_{mech}^2}{JRC^{2.5}} \quad (26)$$

where e =hydraulic aperture for $e/E_{mech} \leq 1$ (with apertures measured in microns); and JRC =joint roughness coefficient. The Barton et al. (1985) relationship was developed for the situation when water was the permeant. As such, it will tend to underestimate e when considering the homogenous fluid model, since a less viscous fluid will be less affected by any frictional effects due to fracture roughness.

Initial attempts at roughness measurement used a semiautomatic Ferranti Coordinate Measuring Machine, as reported in Indraratna et al. (2002). A mathematical approach was adopted to optimize the surface roughness measurement by using as wide a sampling interval as possible. An interval of 2 mm was finally selected such that for a 100 mm long sample, 51 (i.e., N) data points would be recorded.

Bendat and Piersol (1986) suggested that when conducting Fourier series analyses, the number of harmonic frequencies needed to perform an accurate analysis of a particular profile length would require consideration of n_{max} harmonic frequencies, i.e., $n_{max} = N/2 - 1$, where N is the total number of data points in the profile. For the case of a sample of these dimensions, 25 harmonic frequencies should be sufficient to provide a mathematically acceptable replica of the surface. This outcome is similar to the findings expressed by Yang and Di (2001) who proposed that $n_{max} = 20$ was adequate based upon the analysis of their experimental results, although this finding does not accommodate the mathematical constraints as described by Bendat and Piersol (1986).

A Fourier analysis of a recorded set of data points was performed for $n=0$ to n_{max} harmonic frequencies, and the corresponding Fourier coefficients (a_n and b_n) were calculated. By performing a similar analysis on each of the ISRM (1978) standard roughness profiles, a unique relationship between the harmonic frequency power, or Parseval's identity (\bar{y}^2) and each JRC was developed [Eq. (27)]:

Table 1. Summary of Laser Scanning Statistics

Sample	Data points	\bar{E}_{\log} (mm)	Maximum aperture (mm)	Standard deviation
JP05	4999	0.262	2.48	0.251
JP09	5161	0.134	2.35	0.226

$$\bar{y}^2 = \frac{1}{L} \int_0^{2L} \{f(x)\}^2 dx = \frac{a_0^2}{2} + \sum_{n=1}^{\infty} (a_n^2 + b_n^2) \quad (27)$$

The roughness relationship for rock fracture surfaces is complex due to the combination of small and large wavelength roughness functions (ISRM 1978). However, a roughness assessment can be made by comparison of an actual rock surface with the standard roughness profiles. The power-frequency relationship can be studied by calculating \bar{y}^2 and plotting the variable against n for each of the JRC profiles. This shows a unique combination of \bar{y}^2 and n exists for each JRC. It is this uniqueness that allows the assessment of the appropriate JRC. It is reasonable to believe that planar real (i.e., rough) fracture surfaces are a combination of a number of different JRC profiles or roughness wavelengths, i.e., rock fracture roughness in nature tends to be anisotropic. Thus, despite a range of JRC coefficients attributed to a surface, testing (Price 2005) shows it is the average value from the Fourier analysis JRC_F that represents the overall hydraulic or mechanical roughness characteristics. The roughness data estimated for the two test specimens are shown in Tables 1 and 2 and illustrated in Figs. 3 and 4.

Results and Discussion

The results of the high-resolution laser scanning are presented in Figs. 3 and 4. The aperture was calculated at each point as previously described. The 3D wire-frame model of the fracture surface has a stacked contoured layer showing the variation of fracture aperture. The statistical data for both samples are listed in Table 1.

The \bar{E}_{\log} value represents the average mechanical aperture when the fracture is subjected to a confining stress due only to the self-weight of the upper half of the sample, i.e., a fracture normal stress of effectively zero. Thus, \bar{E}_{\log} represents the $\sigma_N=0$ point of a fracture aperture versus normal stress function (Fig. 5). The subsequent points that correspond to nonzero confining stress conditions are a function of the fracture normal stiffness, and must be measured under test conditions.

The key factor when verifying a proposed fluid flow model is to ensure that the change in mechanical aperture of the fracture is known independently of any flow test back calculations of the hydraulic aperture. This is particularly important where a fracture is rough, since the hydraulic and mechanical apertures are not necessarily identical, depending upon the degree of roughness and the permeating fluid properties. In this study, analysis of the clip

gauge readings provides an average measurement of the change in fracture aperture due to the changes in confining stress or the pore fluid pressure, i.e., $E_{\text{clip}} = E_{\text{mech}0} - \delta_N$, where δ_N is the measured clip gauge deformation. The mechanical response of the fractured samples to fracture normal stress is summarized in Fig. 5. In this figure, the calculated average mechanical apertures are normalized with respect to the initial average mechanical aperture (i.e., $\bar{E}_{\log} = E_{\text{mech}0}$) in the form $E_{\text{mech}}/E_{\text{mech}0}$. Sample JP09 showed linear stiffness behavior over the 0 to 2.5 MPa stress range. Sample JP05 can be identified in Fig. 5 by a marked nonlinear deformation, especially over the initial 1.5 MPa of confinement; a linear response was recorded between 1.5 and 3.5 MPa. It seems that a reasonable explanation for the different response of JP05 can be found in the variations in the scale of roughness seen in the different samples, particularly the obvious large scale feature on part of JP05. Sample JP09 fracture surface appeared relatively planar and flat lying. JP05 showed a localized area of greater fracture amplitude, as is plainly seen in Fig. 4(b). The feature, which occupies nearly 30% of the surface introduced considerable scatter in the estimated JRC for each of the fracture profiles, with two broad submodal groups skewed from the average value. This roughness variation would promote the anisotropic distribution of the contact area, which would complicate the fracture stiffness response, and result in the observed nonlinearity.

Two-phase hydraulic testing of the samples using the TPHPTA can deliver large volumes of test data, giving detailed information on the steady-state and transient flow conditions, as illustrated in Figs. 6(a and b). Samples containing fractures with apertures of this order of magnitude achieve steady-state conditions in a matter of a few minutes. Fig. 6(a) presents one of a variety of tests, and describes a test on JP09 that in this instance commenced with a water phase inlet pressure of about 40 kPa; air phase injection pressures were increased stepwise to a final pressure of about 95 kPa. Analysis of the test data using Eqs. (9) and (10) enables the fracture aperture (e_{hom}) corresponding to the homogeneous fluid properties to be evaluated. The calculated value is seen to increase slightly with the air inlet pressure, although the value of the aperture remains within about 10% of the initial magnitude throughout most of the test. There is increased variability in the calculated aperture for air inlet pressures greater than 60 kPa, which is attributed to the onset of higher air velocities and the development of slip under dynamic flow conditions. The same approach can be applied to the data shown in Fig. 6(b), which shows the test response for sample JP05 subjected to a fracture normal stress of 500 kPa and a sustained water phase inlet pressure of about 95 kPa.

The localized increases in calculated aperture are believed to correspond to improved air phase flow path connectivity, which results in this apparent aperture dilation. In reality, no physical increase in aperture would be expected, but rather there has been an improvement in the mixture conductivity due to the increase in phase pressure drop and the reduction in mixture viscosity associated with the reduction in water phase saturation, S_w . The greater variability of the calculated aperture values when $u_a \gg u_w$ is understood to represent the onset of increasing slip con-

Table 2. Comparison of Aperture and Joint Roughness Coefficient (JRC) Values at 500 kPa Confinement

Sample	Average JRC _F	Empirical JRC [Eq. (26)]	e_h (μm)	E_{mech} (μm)	e_{hom} (μm)	E_{clip} (μm)
JP05	9 to 8.5	9.1	75	135 to 126	122	137
JP09	7 to 7.5	7.1	115	122 to 133	121	125

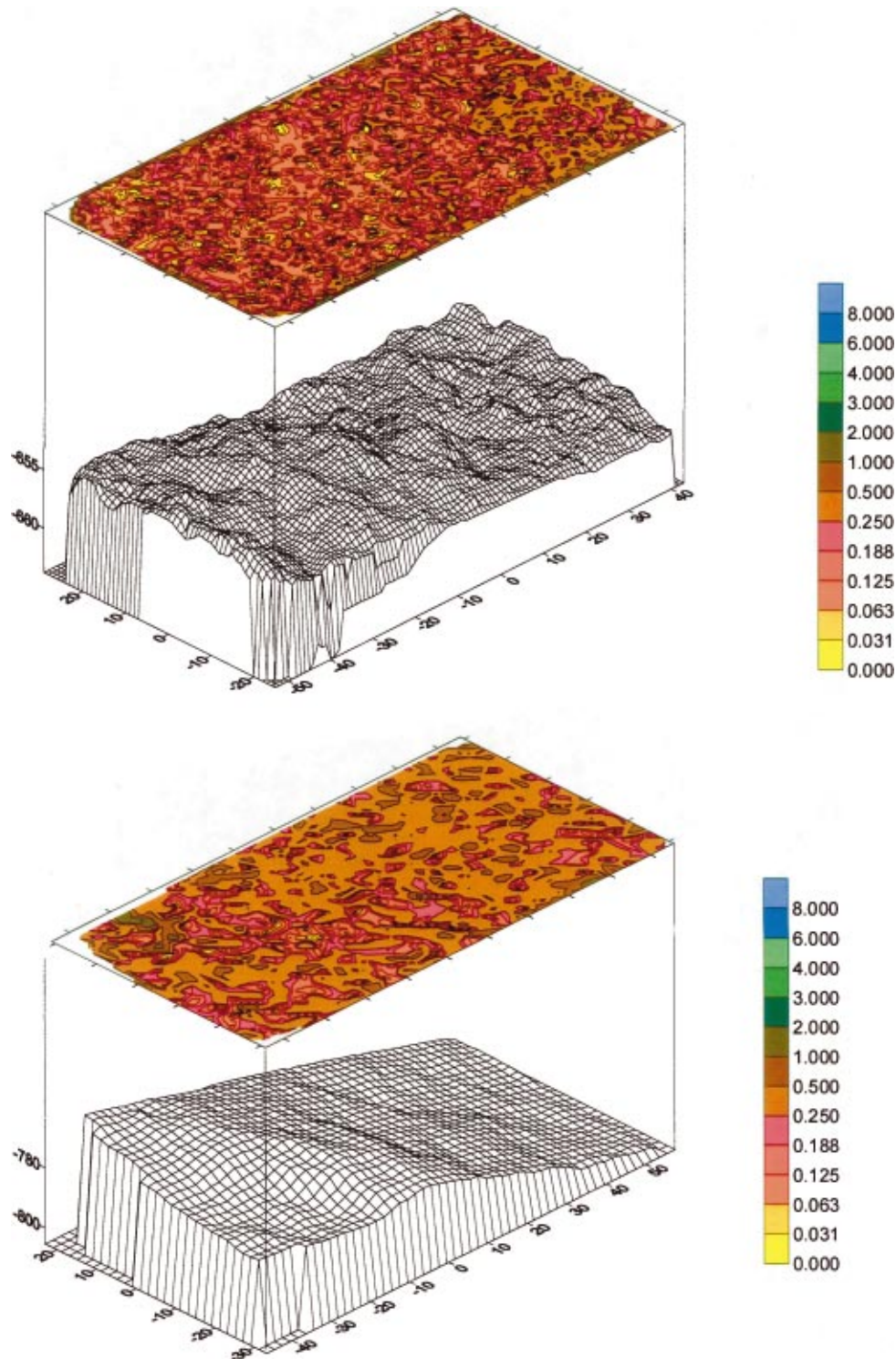


Fig. 4. (Color) (a) Sample JP09 wire-frame surface and contoured aperture distribution data; (b) wire-frame surface and contoured aperture distribution analysis data for Sample JP05, showing large scale waviness in foreground (NB: x , y , and z units all mm)

ditions where the model assumptions are no longer applicable.

Comparison with the laboratory data published by Fourar et al. (1993) suggests that froth and annular two-phase flow patterns tend to deviate from the linear trend that defines laminar flow. Hence, the two-phase flow patterns encountered during this particular testing probably correspond to bubble flow patterns, located within the laminar flow regime, possibly tending to complex or froth patterns at very high air phase test pressures. The

assumed laminar flow conditions appear reasonable if the experimental mixture flow rates are plotted against pressure drop. A sample of the test data is shown in Fig. 7. This graph shows a mainly linear trend occurring during two-phase testing for pressure drops up to 100 kPa.

It is interesting to plot the average calculated e_{hom} values (normalized by the initial mechanical aperture) for each of the fracture normal stresses and to compare them with the measured nor-

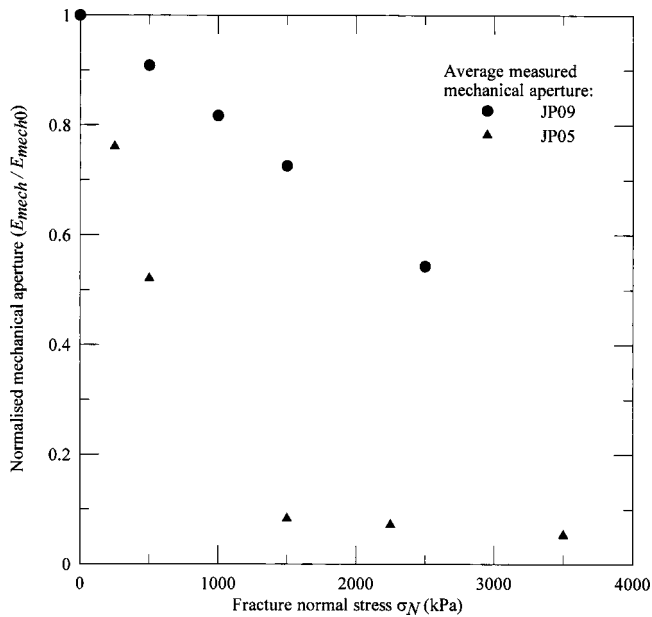


Fig. 5. Change in mechanical fracture aperture with fracture normal stress using clip gauge measurements

malized fracture normal stiffness functions based upon the clip gauge data (Fig. 8). From this plot, there is clearly a strong similarity between the E_{mech} versus σ_N data, and that for e_{hom} versus σ_N . This relationship suggests that the homogenous fluid provides a good technique for assessing rock mass dilation and fracture aperture estimation. It is especially noteworthy that this approach overcomes the single-phase testing problem of increased pressure drop due to fracture roughness, and therefore, over the range of roughness investigated, dispenses with the need for empirical correlation, such as that by Barton et al. (1985). Where both single-phase water and two-phase air-water testing can be applied to the same fracture, this knowledge allows an assessment of the single-phase (water) hydraulic aperture and thus the fracture roughness. Therefore, this additional testing would provide valuable additional hydromechanical rock mass properties using simple testing and calculation.

It is informative to test the validity of the proposed roughness assessment by comparing the homogenous fluid test data and the corresponding single-phase water testing results obtained at a particular confining stress. This information is summarized in Table 2. The assessed JRC_F and the measured single-phase hydraulic aperture e_h are used to calculate the mechanical aperture E_{mech} with Eq. (26). For comparison, the measured mechanical aperture E_{clip} and e_h can also be used to calculate the empirical JRC with the same equation. Table 2 shows that the assessed roughness and the empirical roughness are very similar. In addition, the homogenous fluid aperture e_{hom} is shown to be very close to the measured mechanical aperture, i.e., within 5 to 10%. Improved accuracy and reduced data scatter could be achieved for tighter or rougher fractures through testing with larger datalogger time increments. The e_{hom} value is based upon a range of test results calculated over a range of different pressure gradients yet, despite this, shows acceptable agreement with the measured and calculated values. This outcome gives confidence to the applicability of the proposed JRC assessment technique, since the assessed JRC_F agrees well with the empirical JRC calculated from the single-phase hydraulic aperture e_h and the measured mechanical aperture E_{clip} .

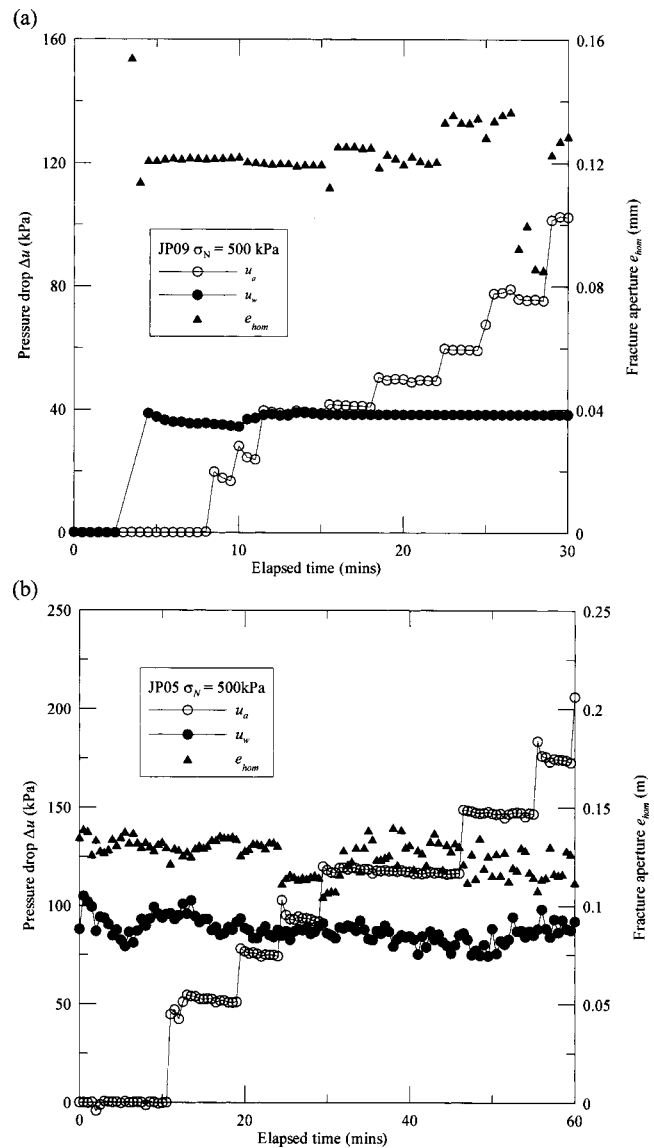


Fig. 6. Two phase test results: (a) sample JP09 confined at 500 kPa with water phase pressure drop 40 kPa; (b) sample JP05 confined at 500 kPa with water phase pressure drop 95 kPa

To extend the $e_{hom} : E_{mech}$ comparison, a graph plotting normalized e_{hom} ($=e_{hom}/E_{mech0}$) versus normalized E_{mech} ($=E_{mech}/E_{mech0}$) was prepared (Fig. 9). The test data for both samples are plotted together. The points plot close (within about 10%) to the 45° line in all cases and confirm the proposition that e_{hom} is a good predictor of E_{mech} .

Conclusions

A simplified coupled homogenous fluid model has been presented to predict pseudo-two-phase flow of air and water mixtures through rock fractures. The suitability of the proposed model has been verified against laboratory data that has been acquired from complicated two-phase flow triaxial testing and from analysis of high-resolution surface roughness investigation of the test specimen fracture surfaces. As part of the triaxial testing, fracture aperture dilation was recorded so that the average dilation could be compared with the predicted “hydraulic” aperture, related to back

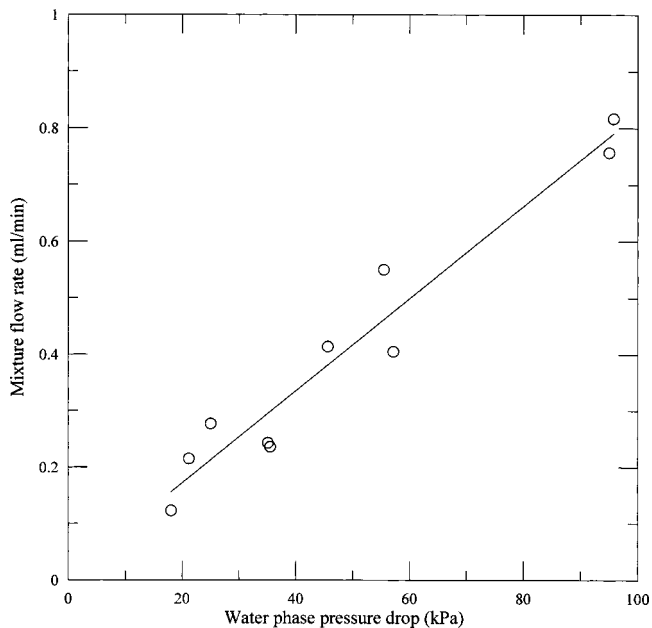


Fig. 7. Selected test data for Sample JP09 showing variation in mixture velocity with water phase pressure drop

analysis of the tests under assumed Darcian conditions. The outcome of this comparison indicated good agreement between calculated aperture (e_{hom}) and the predicted aperture (E_{mech}) based on the physical deformation measurements. It would seem that greater information about the flow behavior could be obtained if the two-phases were considered separately, particularly in terms of the phase saturation and the relative permeability.

The approach that has been described is applicable to the analysis of a single fracture using an adaptation of single-phase flow theory. The approach can also be applied to the analysis of

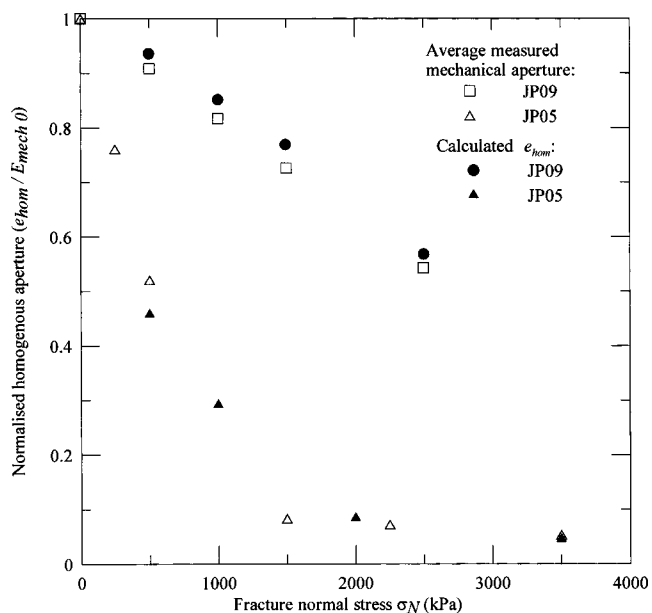


Fig. 8. Comparison of the average calculated homogenous fluid fracture aperture with the recorded fracture dilation data obtained from analysis of the clip gauge readings

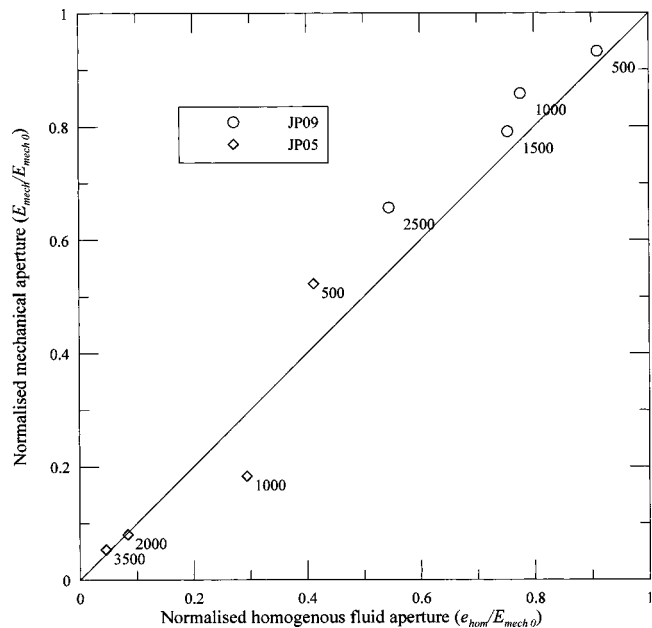


Fig. 9. Plot of normalized homogenous fluid and mechanical apertures for Samples JP05 and JP09. Note: Data points labelled with corresponding fracture normal stress (kPa).

intersecting fracture networks based on simple network analyses, e.g., Priest (1993), provided the pressure gradient, flow boundary conditions, and fracture apertures are known.

The model is limited to laminar flow behavior where there is negligible slip between the phases, i.e., air and water phase velocities approximately equal. The fractures considered in this model are sufficiently wide so that the flow is unaffected by interfacial capillary pressures. The two-phase mixture incorporates air bubbles in a continuous water phase, such that the rough fracture surfaces remain wetted due to surface tension and the small rock matrix pore size.

The homogenous fluid approach applied to fracture hydraulics indicates the results do not seem to be influenced by roughness and flow path tortuosity, where a sufficient volume of air is present, unlike for single-phase water flow. This observation would be expected because the mechanical aperture (E_{mech}) would approximate the hydraulic aperture (e_h) if lower viscosity fluids are used as the permeant (e.g., single phase air testing shows different results to water testing). Further detailed study could show the microscopic (i.e., bubble-scale) two-phase flow behavior, and maybe allow consideration of the inter-relation of mixture viscosity and phase saturation. However, a development of the study along these lines would be more readily dealt with, if separate phases were considered.

It is observed that e_{hom} tends to the physical or mechanical aperture as the relative proportion of the water phase fluid decreases. This shows the potential for this method to be applied to in situ tests, so that the mechanical aperture and fracture roughness could be estimated. This would require small adaptation to existing borehole packer apparatus with the advantage of providing additional important geotechnical data during the investigation stage of a project.

A new technique for fracture profile roughness assessment has been proposed that can be easily calculated using a simple computer program or a set of spreadsheet formulae. The methodology appears applicable over a range of fracture topographies with

specimen JRC_F values assessed between 9 and 7. The JRC_F can be compared to the one that would be predicted from the Barton et al. (1985) relationship. This acceptable agreement between the two results gives confidence in the suitability of the outlined JRC assessment technique.

Laser scanning seems to provide a valuable method of data acquisition of real rock fractures. The technique has the advantage of acquiring high accuracy and high-resolution data. The fine scan interval allows scope for considerable analysis and the fracture aperture can be calculated to a high vertical accuracy. Laboratory testing results for the fracture stiffness and the calculated homogeneous aperture appear to confirm that the average log-normal aperture calculated from the laser scanning data is representative of the fracture mechanical aperture at zero-confining stress. For a smooth fracture, this value is also equivalent to the single-phase hydraulic aperture.

Acknowledgments

Acknowledgement of essential contributions to this research project should include the financial supporters, namely the Australian Research Council (ARC), and Strata Control Technology (SCT). Further assistance was obtained from New Dawn 3D who provided specialist advice on the surface laser scanning of the rock samples, and a special debt of gratitude is owed to the technical staff at the university.

References

- Barton, N., Bandis, S. and Bakhtar, K. (1985). "Strength, deformation, and conductivity coupling of rock joints." *Int. J. Rock Mech. Min. Sci. Geomech. Abstr.* 22, 121–140.
- Bendat, J. S., and Piersol, A. G. (1986). "Random data: Analysis and measurement procedures.", 2nd Ed., Wiley, New York, 566.
- Fourar, M., Bories, S., Lenormand, R., and Persoff, P. (1993). "Two-phase flow in smooth and rough fractures: Measurements and correlation by porous medium and pipe flow models." *Water Resour. Res.* 29:11, 3699–3708.
- Fredlund, D. G., and Rahardjo, H. (1993). *Soil mechanics for unsaturated soils*, Wiley, New York, 571.
- Indraratna, B., and Haque, A. (1999). "Triaxial equipment for measuring the permeability and strength of intact and fractured rocks." *Geotechnique*, 49(4), 515–521.
- Indraratna, B., Price, J., and Gale, W. (2002). "Fourier description of fracture roughness." *Proc., 5th North American Rock Mechs Symp.*, Hammah et al., eds., University of Toronto Press, Toronto, 35–44.
- Indraratna, B. and Ranjith, P. (2001a). *Hydromechanical aspects and unsaturated flow in jointed rock*, A. A. Balkema, Lisse, 286.
- Indraratna, B., and Ranjith, P. G. (2001b). "Laboratory measurement of two-phase flow parameters in rock joints based on high pressure triaxial testing." *J. Geotech. Geoenviron. Eng.* 127(6), 530–542.
- Indraratna, B., Ranjith, P. G., Price, J. R., and Gale, W. (2003). Two-phase (air and water) flow through rock joints: Analytical and experimental study." *J. Geotech. Geoenviron. Eng.*, 129(10), 918–928.
- International Society for Rock Mechanics (ISRM). (1978). "Suggested methods for the quantitative description of discontinuities in rock masses. Part 1." *Site characterization, rock characterization testing and monitoring*, ISRM Suggested Methods. E. T. Brown, ed., Commission on Testing Methods, Pergamon, N.Y.
- McAdams, W. H. (1942). "Vaporization in horizontal tubes II benzene—Oil mixtures." *Trans. ASME* 64, 163 [cited in Wallis G. B., (1969)].
- Persoff, P., and Pruess, K. (1993). "Flow visualisation and relative permeability measurements in rough walled fractures." *Proc., 4th Annual Int. High Level Radioactive Waste Management Conference*, American Nuclear Society, La Grange Park, Ill., 2033–2041.
- Price, J. (2005). "Coupled two-phase air and water flow in rough fractures." PhD thesis, Univ. of Wollongong, Wollongong City, New South Wales, Australia.
- Priest, S. D. (1993). *Discontinuity analysis for rock engineering.*, Chapman-Hall, London, 473.
- Vennard, J. K., and Street, R. L. (1982). *Elementary fluid mechanics*, 6th Ed. Wiley, New York, 689.
- Wallis, G. B. (1969). *One-dimensional two-phase flow*, McGraw-Hill, New York, 408.
- Witherspoon, P. A., Wang, J. S. Y., Iwai, K., and Gale J. (1980). "Validity of cubic law for fluid flow in a deformable rock fracture." *Water Resour. Res.*, 16(6), 1016–1024.
- Yang, Z. Y., and Di, C. C. (2001). "A directional method for directly calculating the fractal parameters of joint surface roughness." *Int. J. Rock Mech. Min. Sci.* 38, 1201–1210.